Research Article

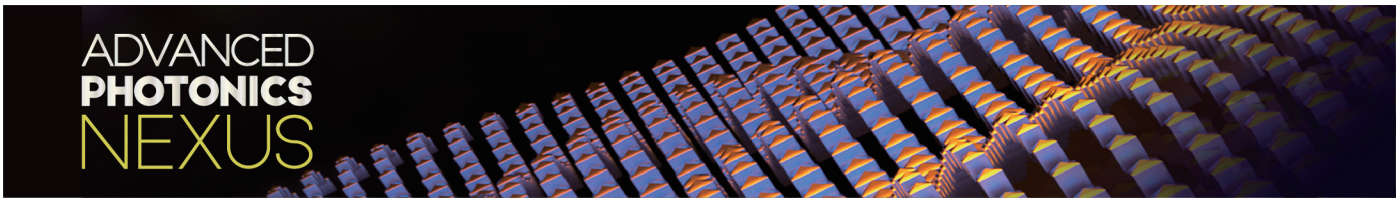

Terahertz probe for real time *in vivo* skin hydration evaluation

Arturo I. Hernandez-Serrano,[a] Xuefei Ding,[a] Jacob Young,[a] Goncalo Costa,[a] Anubhav Dogra,[a] Joseph Hardwicke,[b,c] and Emma Pickwell-MacPherson[a,*]

[a]University of Warwick, Department of Physics, Coventry, United Kingdom
[b]Warwick Medical School, University of Warwick, Coventry, United Kingdom
[c]Institute of Applied and Translational Technologies in Surgery, University Hospitals Coventry and Warwickshire NHS Trust, Coventry, United Kingdom

Abstract. This study introduces a handheld terahertz (THz) scanner designed to quantitatively evaluate human skin hydration levels and thickness. This device, through the incorporation of force sensors, demonstrates enhanced repeatability and accuracy over traditional fixed THz systems. The scanner was evaluated in the largest THz skin study to date, assessing 314 volunteers, successfully differentiating between individuals with dry skin and hydrated skin using a numerical stratified skin model. The scanner measures and displays skin hydration dynamics within a quarter of a second, indicating its potential for real-time, noninvasive examinations, opening up opportunities for *in vivo* and *ex vivo* diagnosis during patient consultations. Furthermore, the portability and ease of use of our scanner enable its widespread application for *in vivo* and *ex vivo* diagnosis during patient consultations, potentially allowing *in situ* biopsy evaluation and elimination of histopathology processing wait times, thereby improving patient outcomes by facilitating simultaneous tumor diagnosis and removal.

Keywords: terahertz; real time; stratum corneum; hydration; *in vivo diagnosis*; noninvasive examination.

Received Sep. 6, 2023; revised manuscript received Dec. 21, 2023; accepted for publication Dec. 27, 2023; published online Feb. 5, 2024.

[DOI: 10.1117/1.APN.3.1.016012]

1 Introduction

The outermost layer of skin, the stratum corneum (SC), maintains the skin barrier function, plasticity, and normal process of desquamation. Disrupting SC hydration may result in several dermatological conditions, for example, eczema and atopic dermatitis.[1,2] Therefore, there is a strong need for noninvasive, accurate, and real-time quantitative monitoring of skin hydration and thickness.

Existing techniques for monitoring skin hydration include evaporimetry, which measures transepidermal water loss (TEWL), electrical-based methods (corneometry), optical-based methods [optical coherence tomography (OCT)], and nuclear magnetic resonance (NMR).[3–6] The limitations of evaporimetry and corneometry are that they are easily influenced by extrinsic and intrinsic factors. For example, room temperature and ambient humidity can alter the TEWL results, and substances other than water in the skin may have an effect on the skin impedance. NMR and OCT can provide clear images of skin layers and acquire multiple properties, including SC thickness and water concentration gradient; however, the instrumentation is often large and/or expensive, and often only able to measure a limited range of locations on the human body.

Terahertz (THz) light is nonionizing radiation in the frequency range of 0.1 to 10 THz (1 THz $= 10^{12}$ Hz). THz light is highly sensitive to the presence of water, given the high absorption coefficient (200 cm^{-1} at 1 THz).[7] Studies have revealed the potential of utilizing THz spectroscopy and imaging for *ex vivo* investigations of excised biological tissues, including breast cancer,[8,9] skin cancer,[10,11] colon cancer,[12] and dental caries.[13] There have also been demonstrations of *in vivo* THz imaging of diabetic foot syndrome,[14] pigmentary skin nevi,[15] corneal tissue water content,[16] burn wounds,[17] skin flaps,[18] and healthy skin under different hydration statuses.[19–21] Evidence from magnetic resonance imaging studies has shown that tumor areas have increased water content compared with healthy ones[22,23] and so findings related to skin hydration could well

*Address all correspondence to Emma Pickwell-MacPherson, e.macpherson@warwick.ac.uk

be applied to cancer detection, making THz light a potential candidate for the evaluation of skin diseases. These studies mostly employed conventional THz time-domain spectroscopy (THz-TDS) systems set up in reflection geometry due to the high absorption of biological tissue.[10,24,25]

Different handheld THz scanners have been proposed to carry out reflection measurements.[26–29] Recently, Harris et al. developed a THz portable handheld spectral reflection scanner for fast THz imaging in 0.25 to 1.25 THz with a field of view of 12 mm × 9 mm; it was applied in the assessment of burn wounds on a porcine model.[30,31] However, none of the aforementioned systems keep control of the contact force between the scanner and the skin, which is crucial, given that the compaction of skin layers can induce alterations in water distribution within the skin, yielding a perceived increase in water content and reduced thickness.[20]

In this work, we present our handheld THz scanner with incorporated force sensors suitable for point-scan *in vivo* measurements of skin in reflection geometry. We compare our proposed scanner with two robust but bulkier systems to demonstrate the reliability of the portable handheld instrument. We then use the handheld scanner to conduct the largest hitherto *in vivo* THz study (of 314 individuals) in an out-of-lab environment. Furthermore, we present a numerical model based on a stratified media framework for the computation of SC hydration and thickness. This model gives us the capability to investigate the influence of the aforementioned skin properties on the reflected THz pulse. The robustness and accuracy of the handheld THz scanner pave the way for future clinical applications of THz sensing both in the evaluation of skin conditions and for monitoring the efficacy of skin moisturizers used in cosmetics and medicine.

2 Materials and Methods

2.1 Participant Information

The study was approved by the Biomedical & Scientific Research Ethics Committee at Warwick University, BSREC (REGO-2018-2273 AM05). Volunteers participating in the study gave their informed and signed consent. Before our study, the participants completed a questionnaire about their skin type, exercise routine, and water consumption, as detailed in the Supplementary Material. A total of 314 volunteer measurements were made.

2.2 Skin Measurements Using a Microscopic Camera

In our prior research, we conducted a comparative study between THz sensing and both a corneometer and TEWL. Our findings demonstrated that the corneometer reading exhibited a decreased efficacy in distinguishing variations in skin hydration compared to a THz measurement and generally lacks accuracy and reliability.[32] Similarly, TEWL quantifies the volume of water vapor emanating from the skin within a specific period of time in grams per square meter. High readings indicate greater water loss measurements, making the technique indirect and only suitable for skin surface information. In this previous study, we also took a photo of the skin with a microscopic camera, and we use this camera again in this study to help demonstrate the sensitivity of the THz scanning. For each participant, the area of skin to be THz scanned was photographed prior to measurement using a USB microscopic camera. A set of photos of 12 different volunteers with dry skin and normal skin is presented in the Supplementary Material and shows the drier skin has more defined ridges.

2.3 Handheld THz Scanner for In Vivo Skin Measurement

Our handheld THz probe is based on the TeraSmart THz time-domain spectrometer from Menlo Systems. The THz emitter and detector are mounted in the probe head to obtain an oblique reflection geometry with an incident angle of 30 deg, as illustrated in Fig. 1(a). The THz photoconductive (PC) emitter delivers a train of broadband electromagnetic pulses with a time duration of a few picoseconds and is detected by another PC antenna. A typical THz pulse emitted by our system and reflected off a gold mirror is shown in Fig. 1(b). The spectrum of the THz pulse is shown in Fig. 1(c). The spectral bandwidth of this typical pulse ranges from 0.1 to 4 THz with a dynamic range of around 75 dB and a central frequency of 0.7 THz. It is noteworthy that the signal-to-noise ratio at 0.1 THz, ∼20 dB, surpasses the 75 dB noise floor, thereby substantiating the presence of said frequency within the spectra.

The basic operation of the handheld scanner is illustrated in Fig. 1. For skin measurements, the quartz window of the probe is placed onto the volunteer's skin. The purpose of the quartz window is to flatten the skin as well as to keep it in focus. The refractive index of the quartz is $n_{qz} = 1.95 - 0.0048i$.[33] The two reflections of the THz beam from the quartz window are shown in Fig. 1(e). The first reflection (A), from the air–quartz interface, is used to align the measured reflections, as they can be slightly shifted due to fiber optic drift and small mechanical deformations of the scanner. The second reflection (B) from the quartz–skin–air interface contains sample information when the skin is measured, or reference information if air is measured. Note, the reflection at B is in focus and therefore has a higher amplitude than the reflection at A, which is not in focus. To ensure meaningful comparisons and allow for any THz signal fluctuation, the THz pulses are processed to extract the impulse function of the sample, calculated as

$$\mathrm{Im\,pulse}(t) = \mathrm{FFT}^{-1}\left\{\frac{\mathrm{FFT}[E_{\mathrm{samp}}(t)]}{\mathrm{FFT}[E_{\mathrm{ref}}(t)]}\right\}, \tag{1}$$

where $E_{\mathrm{samp}}(t)$ and $E_{\mathrm{ref}}(t)$ are the THz pulse reflected from skin and air, respectively. More details are given in Ref. 34. The THz system operates at an acquisition rate of 15 Hz within a time window of 50 ps. However, signal acquisition is performed using our in-house software, which computes the refractive index, absorption coefficient, impulse function, and reflectance with each acquisition. These computations necessitate a certain processing time, resulting in the handheld scanner effectively recording and processing four pulses per second (4 Hz). This operational speed is deemed sufficient for capturing variations in skin hydration attributed to occlusion. Consequently, our system facilitates the real-time assessment of water accumulation in the skin.

To carry out the *in vivo* examinations, the handheld scanner is placed on the volar forearm of the volunteer, as illustrated in Fig. 1(f). Furthermore, two force-sensitive resistors are fixed next to the quartz window, as shown in Fig. 1(g) to measure the force exerted on the skin over the area of the probe head (resulting in pressures between 0.6 to 1.1 Ncm^{-2}[34]). This

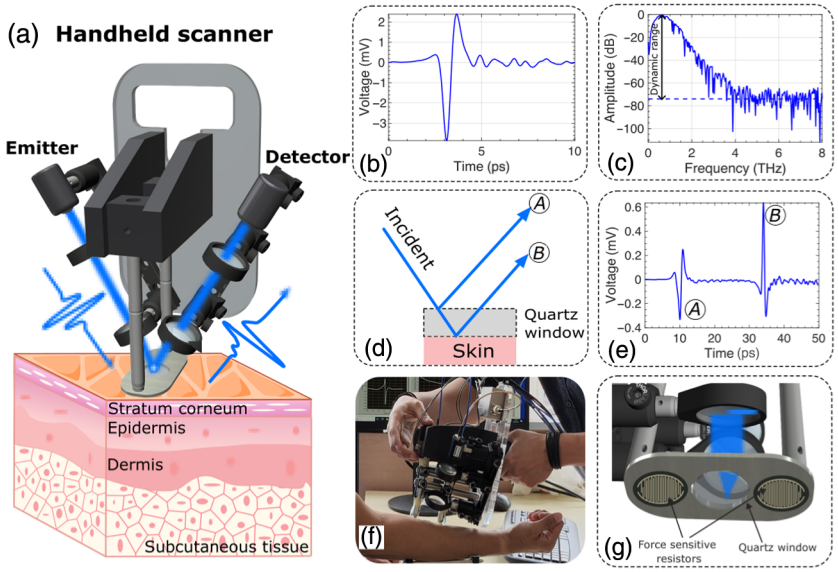

Fig. 1 The portable THz handheld scanner. (a) Handheld system and skin diagram. (b) A single raw THz reference signal reflected from a gold mirror and the result of averaging 20 pulses. (c) Fourier spectra indicating that averaging increases the dynamic range by over 10 dB. (d) Diagram illustrating the two reflections of the THz pulse, one from the air–quartz interface labeled as "*A*," and one from the quartz–skin–air interface labeled as "*B*." (e) Example of a typical THz-TDS trace reflected from the interface air–quartz (*A*) and quartz–skin (*B*). (f) Photograph of the handheld probe scanning the volar forearm of a volunteer. (g) Two force-sensitive resistors are fitted on the tip of the probe to ensure consistent force applied onto the skin for every measurement.

strategy ensures equal and consistent pressure during measurements, preserving repeatability.

2.4 Comparison of the Portable THz Handheld Scanner with Two Fixed Platform Systems

Our handheld scanner was compared with two other robust but bulkier systems. These systems each have a 2 mm thick quartz window fixed to a platform, and the volunteer places their arm on top of the quartz window and force sensors. The THz beam is approximately elliptical with axes 5 and 10 mm, and the acquisition rate is set to 4 Hz. The force sensors are next to the window on the imaging platform, and the volunteer (rather than the operator of the handheld probe) controls the contact pressure. The three systems are illustrated in Figs. 2(a)–2(c). The dielectric properties of the volar forearm of 10 different volunteers were calculated using the three systems and compared for volunteer 1 in Figs. 2(d)–2(f). The refractive index results of the volar forearm of the other nine volunteers (volunteers 2 to 10) acquired with the three systems are given in the Supplementary Material. The mathematical analysis for the calculation of the complex refractive index from reflected THz pulses from the skin is detailed in our previous work.[34] Excellent agreement among the three systems is found and, impressively, a reduced uncertainty is observed for the handheld scanner. This is because the operator controls the pressure, combined with the enhanced stability of the setup from the stronger caging, preventing mechanical deformations and misalignment when the system is pressed against the skin. The act of placing the quartz window of the handheld system on the skin causes water to start accumulating on the surface of the skin. This phenomenon is well known as the "occlusion effect" and reflects the accumulation of hydration in the skin by porous obstruction.[34] The increased water in the skin leads to an increase in its refractive index, reducing the difference between the refractive index of the quartz window and the skin. This reduced mismatch in a refractive index reduces the amplitude of the reflected signal. Thus, during the measurement, the amplitude of the recorded impulse function is observed to decrease as function of time as shown in Fig. 3(a), where the pulses have been shifted horizontally for better clarity. The calculation of the impulse function was done for the frequency range between 0.1 and 0.7 THz.

The results in Fig. 2 are calculated from the final 5 s (between 55 and 60 s of occlusion) of each subject's measurement (20 THz pulses), as the change in the skin response due to occlusion decreases significantly after about 30 s of contact; this gives a way to compare the three systems' performances. In the measurements of volunteer 1, system 1 systematically gives a higher value than the other systems. This was not always the case, but it was often offset either above or below the other two systems for the other nine volunteers as shown in Fig. S4 in the Supplementary Material, and consistently had larger error bars, suggesting it is harder to control the contact pressure in system 1.

The peak-to-peak (P2P) amplitude, which is the difference in amplitude between the highest and lowest points of a waveform, is plotted in Fig. 3(b) for 60 s duration of the measurement for seven different volunteers (dots) together with the corresponding bi-exponential fittings (continuous lines). These results, subsequently referred to as occlusion curves, were selected to illustrate the range of responses observed. Interestingly, the occlusion curves for the different volunteers present different

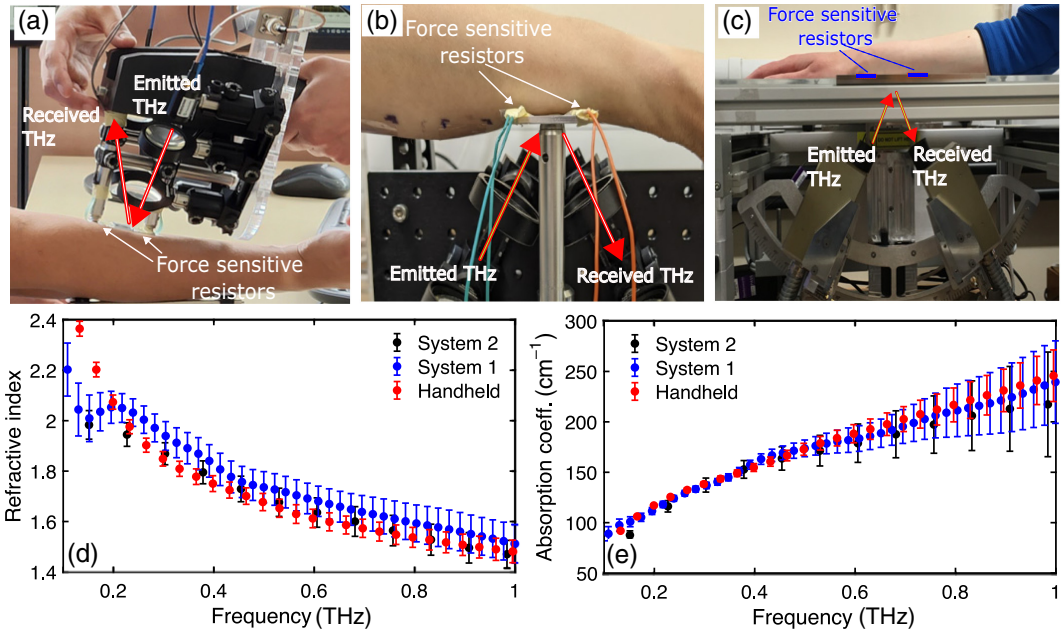

Fig. 2 Comparisons of the three systems and their corresponding measurements of volunteer 1. Photos of the actual systems scanning the volar forearm of a volunteer. (a) Proposed handheld probe, (b) system 1 (Menlo K15) with a fixed window platform, and (c) system 2 (TeraView TPS4000 Gantry system). (d) The refractive index and (e) absorption coefficient results for volunteer 1 from the handheld probe (red dots), system 1 with a fixed window platform (blue dots), and system 2 (black dots). The results shown are the average of 20 measurements (dots) from between 55 and 60 s of occlusion and the corresponding standard deviation (error bars).

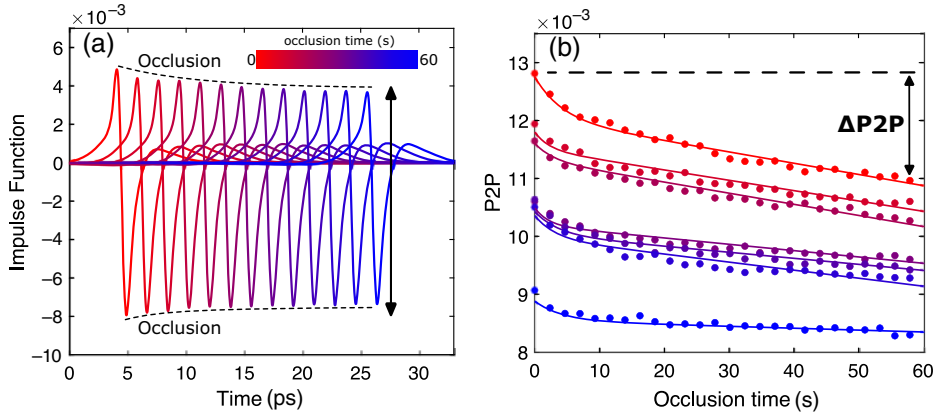

Fig. 3 Experimental occlusion curves obtained with the handheld system. (a) Impulse function recorded during 60 s of measurements from the volar forearm of a single volunteer. The pulses have been offset horizontally for clarity. The P2P amplitude decays as a function of recording time due to the occlusion effect. (b) P2P curves (occlusion curves) and their bi-exponential fit (dots and continuous lines, respectively) of seven different volunteers highlighting the variation across volunteers. The definition of ΔP2P is given as the vertical difference between the first and last point on the occlusion curve and is an indicator of hydration. The color bar indicates the occlusion time for the corresponding data plotted.

vertical offsets and decay rates (ΔP2P). The decay rate is calculated as the difference in the P2P amplitude after measuring for 60 s (compared to the first measurement taken). In Fig. 3(b), it is clear that ΔP2P changes depending on the vertical position of the occlusion curve. The higher the initial vertical location of the curve is, the higher the ΔP2P value is. This fact potentially provides us with information about the state of the skin during measurements.

2.5 Modeling the Skin Response to Understand the Changes in Occlusion Curve

To analyze the skin response under THz light, a numerical model of the skin is used to simulate the skin under different hydration conditions. An approximated water profile of skin as a function of depth obtained from previous studies using Raman spectroscopy is shown in Fig. 4(a).[35,36] In our case, this hydration profile is completely defined by three parameters: skin surface hydration ($H0$), epidermis hydration ($H1$), and SC thickness (d). This water distribution applied in an effective-medium model is capable of calculating the effective dielectric properties of the skin as a function of depth. Afterwards, these dielectric properties are utilized in a multilayer electromagnetic model to calculate the THz response of the skin. By changing the initial values of $H0$ and d, it is possible to study the dependence of the P2P as a function of the initial hydration state of skin as well as the thickness of the SC, as shown in Figs. 4(b)–4(e). The derivation of our theoretical model is given in the Appendix. From our simulations, we observe that the occlusion effect is mainly given by the change in hydration in the SC rather than the epidermis; this is depicted in Figs. 4(b) and 4(c). To test the effect of initial surface hydration ($H0$), the quantities $H1$ and d were kept constant at 70% and 15 μm, respectively, as they are not expected to change considerably during the 1 min of the test.[35] From Fig. 4(d), it is clear that the initial hydration state of skin [$H0_{ini}$ in Fig. 4(b)] has a strong impact on the value of ΔP2P, with small values of ΔP2P indicating more hydrated

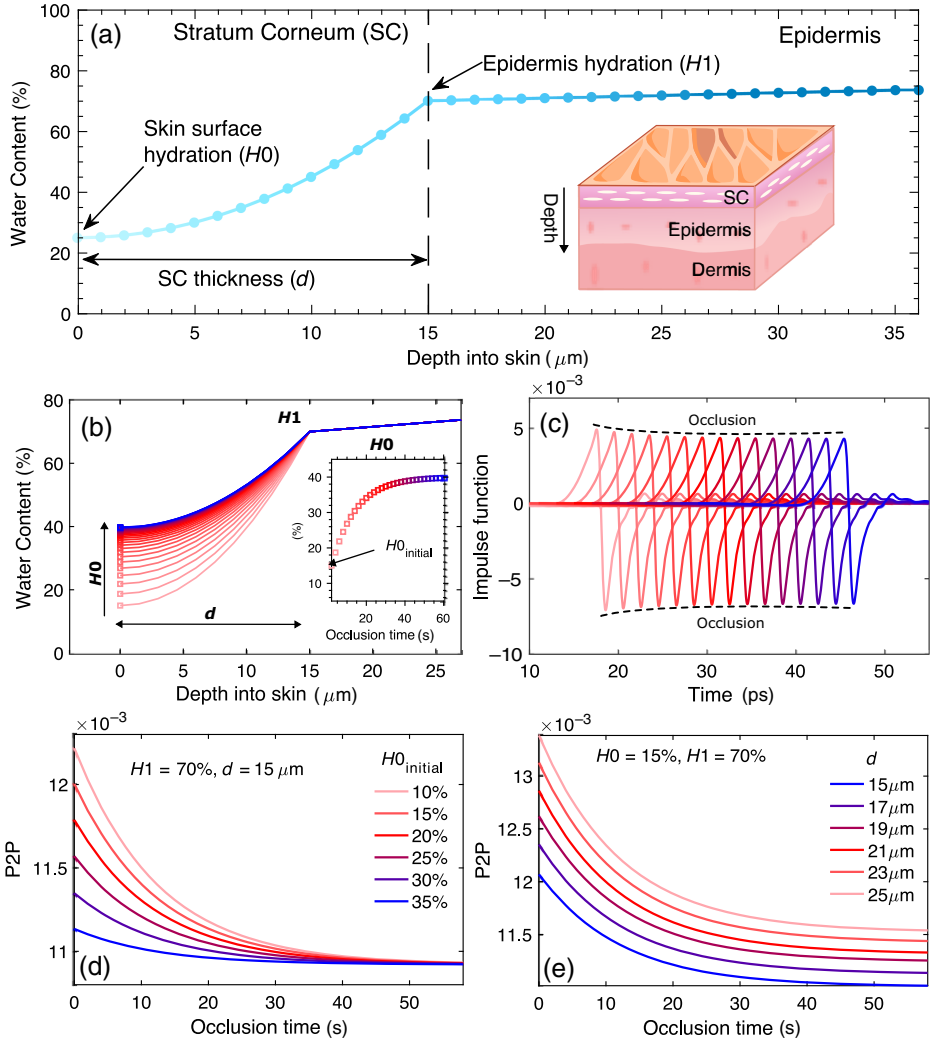

Fig. 4 (a) The water profile distribution follows a quadratic increase in the SC and a linear increase within the epidermis. The parameters $H0$, $H1$, and d characterize this water profile. (b) Simulated water distribution by varying the $H0$ parameter as a function of time following a bi-exponential curve (inset figure) to simulate the occlusion effect for 60 s. (c) Simulated THz pulses using the hydration profiles shown in panel (b). The pulses have been offset horizontally for clear visualization. (d) Simulated occlusion curves when the parameter $H0_{ini}$ is varied from 10% to 35% to simulate skin with different initial hydration conditions, while $H1$ and d have been kept constant at 70% and 15 μm, respectively. (e) Simulated occlusion curves when the parameter d varies from 15 to 25 μm, while $H0$ and $H1$ have been kept constant at 15% and 70%, respectively. The main effect of the thickness of SC is the vertical offset of the occlusion curve.

skin. Finally, in Fig. 4(e), the dependence of the P2P amplitude on the SC thickness (d) is studied by keeping the parameters $H0$ and $H1$ constant at 15% and 70%, respectively. The main effect of d is that the thicker the SC is, the higher the vertical offset is. These results enlighten many of the features observed experimentally in Fig. 3(b). By solving a nonlinear optimization problem of the form,

$$\min \|X_{\text{exp}}(t) - X_{\text{theo}}(H0, H1, d, t)\|_2^2, \tag{2}$$

where $X = \frac{E_{\text{sample}}}{E_{\text{reference}}}$ and $E_{\text{reference}}$ is the THz pulse in the absence of sample. $X_{\text{theo}}(H0, H1, d, t)$ is the theoretical THz pulse given by Eq. (6) in the Appendix. This numerical model is used to characterize the skin on the volar forearm of 314 volunteers with different skin tones, ethnicities, and skin conditions. The nonlinear least square routine used is robust when the initial values and the searching boundaries for $H0$, $H1$, and d are within the values of SC hydration, thickness, and epidermis hydration normally measured using complementary techniques such as Raman and OCT. We used SC thickness: 15 to 35 μm, SC hydration: 5% to 40%, and epidermis hydration: 60% to 70%. Discrepancies in optimized values are occasionally generated by noise in the system, pulse shifting, or misalignments. However, these discrepancies are easy to identify and discard, as they take values at the edge of the searching boundaries.

3 Results

3.1 Dynamic Hydration Profile of Skin

This study represents the largest scale study to date using THz light for skin examination (314 volunteers) and demonstrates the robustness of our proposed instrument. In Fig. 5(a), the scatterplot in a three-dimensional (3D) space is shown. The coordinates in this 3D space are: P2P amplitude at 50 s in the occlusion curve (P2P_{50}), SC thickness (d), and skin surface hydration ($H0$).

For a better understanding of the data, the projection of the cloud of points on each axis is presented in Figs. 5(b)–5(d). Three different colors are employed in the scattered plot to represent questionnaire responses: green for volunteers who did not state that they have dry skin, referred to as "normal" hereafter, red for dry skin, and blue for volunteers with dry skin who used moisturizer before the test. We categorized the participants

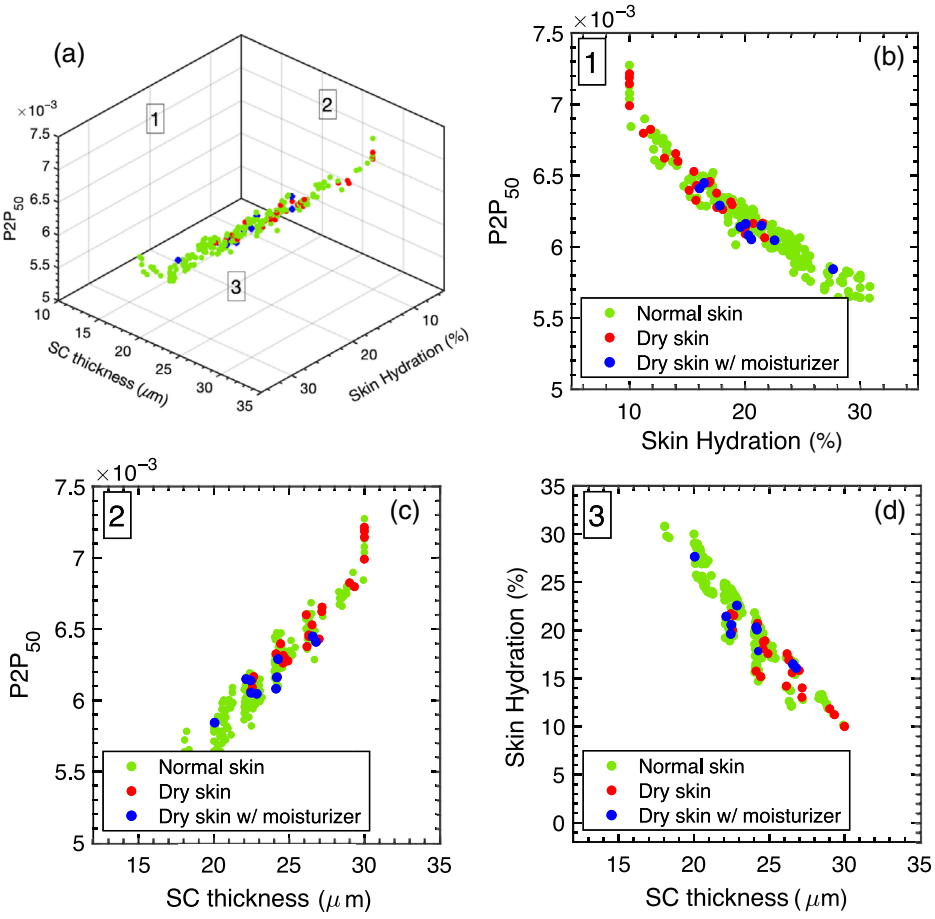

Fig. 5 Scatterplots of the data. (a) Cloud of points of the participants who answered to have normal skin, dry skin, and dry skin being treated with moisturizer. (b) P2P_{50} versus skin hydration for all the participants. (c) P2P_{50} versus SC thickness. (d) Skin hydration ($H0$) versus SC thickness. Different colors have been employed for volunteers with normal skin (green), dry skin (red), and dry skin previously treated with moisturizer (blue). In all the cases, a clear clustering of people with dry skin is observed. Meanwhile, treated dry skin exhibits similar trends as normal skin.

based on their answers in the survey. The scattered dots of the dry skin participants tend to cluster in the upper left corner of Fig. 5(b); most of them have under 20% hydration while the normal skin volunteers are spread out in a wider area; however, both of them exhibit a broadly linear dependence on hydration. Interestingly, the P2P values decreased as a function of surface hydration. This dependence has been previously seen in Fig. 3(b) and is also predicted by our numerical simulations.

In Fig. 6, the differences between the self-diagnosed dry skin participant population (with no moisturizer applied) and normal

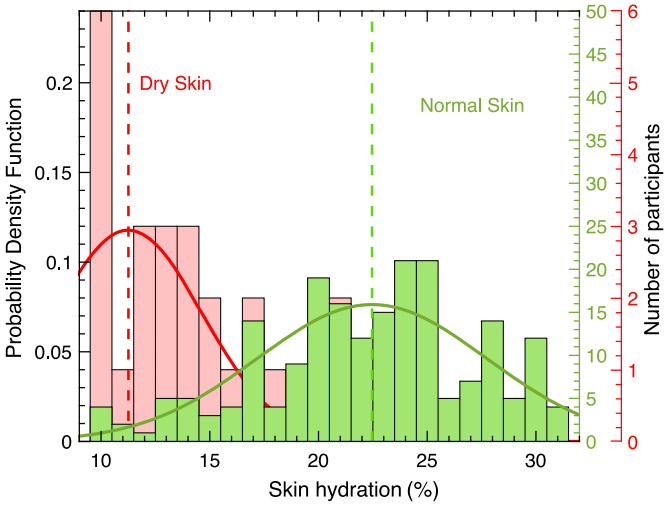

Fig. 6 Histogram showing the number of participants at each skin hydration for dry (red) and normal (green) skin participants (shaded bar chart, axes RHS). The probability density functions (solid lines, axis LHS) are calculated for dry (red) skin and normal (green) skin. The mean hydration values for each group are indicated by the vertical dashed lines.

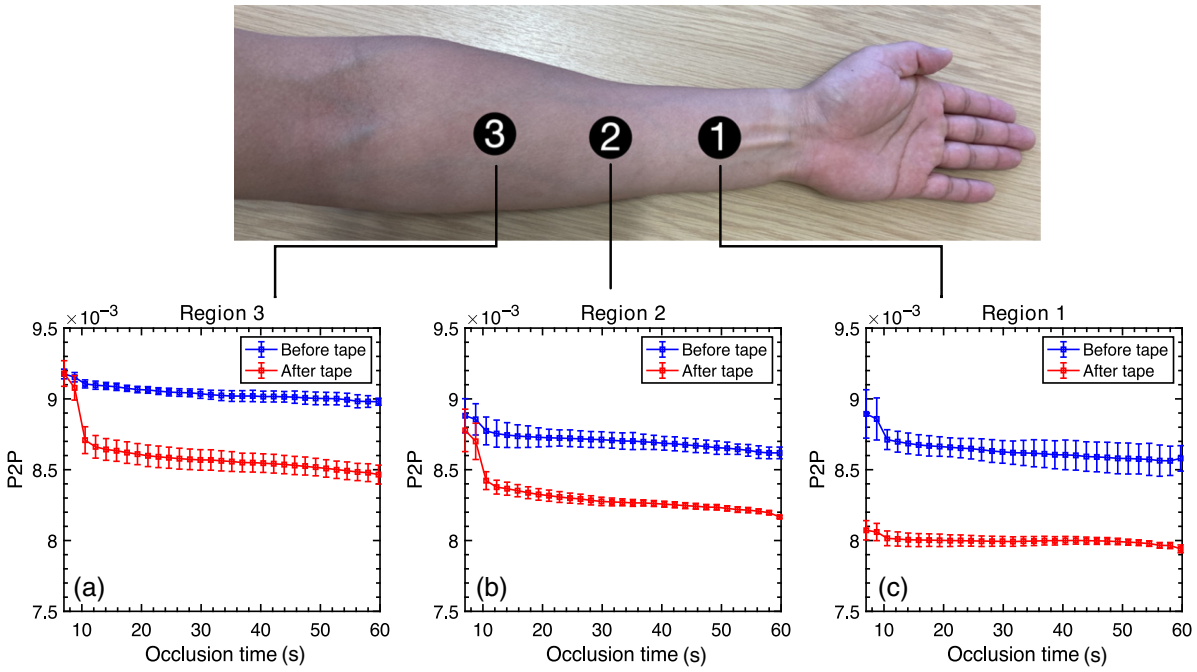

Fig. 7 Effect of the change of the SC thickness on the occlusion curve. Three regions on the volar forearm of a volunteer are measured in panels (a)–(c) before (blue squares) and after (red squares) the reduction in the SC thickness using the tape stripping method. The reduction of the SC thickness is seen as a vertical down offset in the position of the occlusion (P2P) curve. The three regions are each measured 4 times, the squares represent the mean values, and the error bars show the standard deviation.

participant population are highlighted. There is some overlap between the two population distributions, as expected due to the natural variation of skin hydration levels in the population and because the groups are classified by the survey responses. Note that the normal skin population had 220 participants and the dry skin population who had not moisturized had 25 participants. After running a Student's t-test and despite the smaller sample size of the dry skin group, the mean skin hydration of the dry skin population is statistically significantly lower than the normal skin population with a p-value of 2.46%. The range for the participants with dry skin is from 10% to 22%, with 87% of the participants having skin hydration below 20%. In contrast, the range for the normal skin participants is from 10% to 31%, with 52% having a skin hydration above 20%.

3.2 SC Thickness Assessment

We now further validate the model results by conducting a tape stripping experiment to remove the outermost layer of skin cells. Tape stripping is commonly used for the investigation of SC thickness.[35] Figure 7 shows the occlusion curves of three different regions on the volar forearm measured before and after tape stripping. The mean values and standard deviations were calculated for each region; the SC hydration and thickness calculated

Table 1 SC hydration and thickness before and after the application of the adhesive tape.

	Before tape stripping		After tape stripping	
Location	Hydration (%)	Thickness (μm)	Hydration (%)	Thickness (μm)
1	27.03 ± 2.22	24.00 ± 0.04	38.50 ± 2.33	21.89 ± 0.08
2	26.85 ± 0.43	24.80 ± 0.88	32.55 ± 1.35	22.96 ± 0.05
3	23.07 ± 0.72	25.97 ± 0.02	30.07 ± 2.36	23.52 ± 0.25

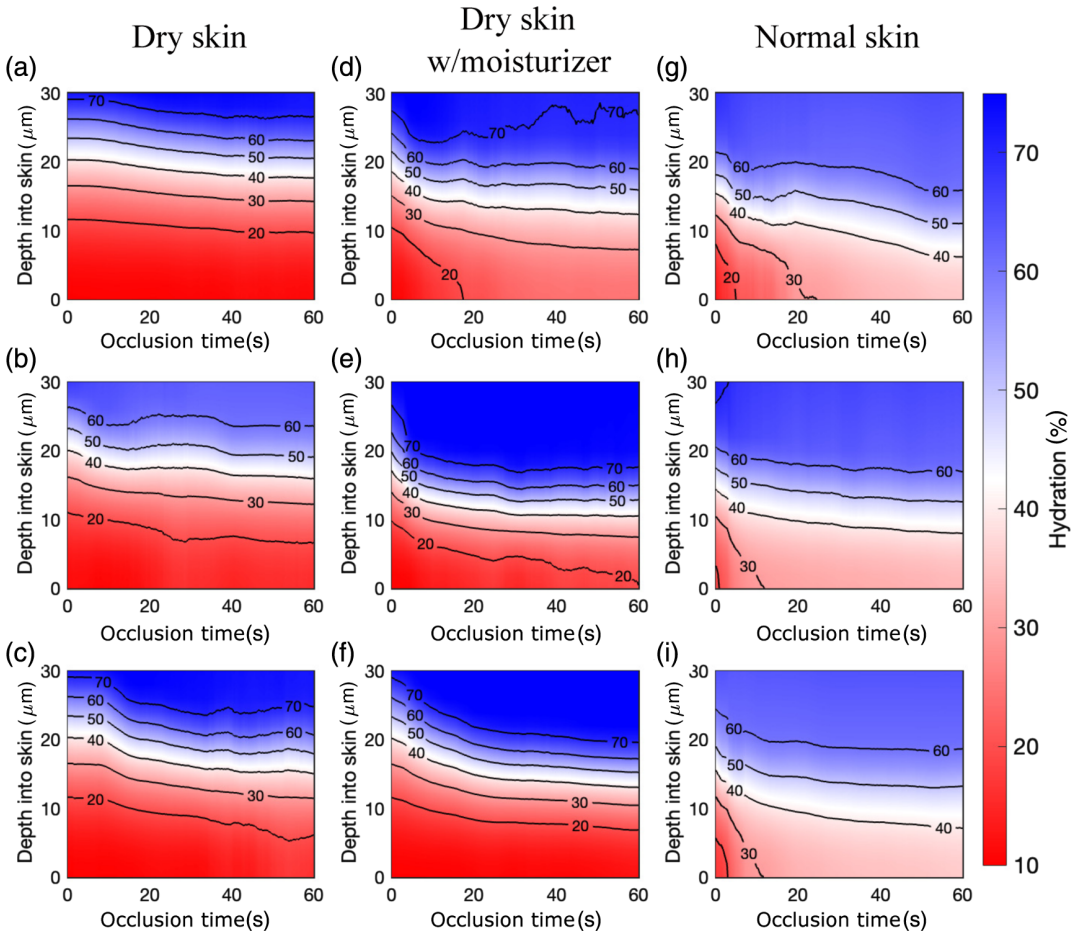

Fig. 8 Accumulation of water as a function of depth into the skin and occlusion time in the skin for nine different volunteers. (a)–(c) Three with normal skin, (d)–(f) three exhibiting dry skin, and (g)–(j) three with dry skin previously treated with moisturizer. Higher hydration levels are found closer to the surface for normal skin at the beginning of the measurement starting at values close to 20%, while for dry skin the initial values are below 20%.

from these data are given in Table 1. The act of tape stripping removes the outer layer of the SC, reducing the thickness. As expected from the modeling, this causes the vertical shift in the occlusion curve seen in Figs. 3(a)–3(c). Similarly, since the outermost layer of the SC is the driest, the $H0$ of the remaining skin being measured is higher, and so we expect the ΔP2P to be reduced. This is also seen in Fig. 4(e), confirming our previous numerical results.

Another observation is that the occlusion curves of participants with dry skin using moisturizer tend to be lower than those with dry skin: the lower P2P indicates higher hydration levels. In Fig. 5(c), the P2P versus SC thickness (d) exhibits an upwards linear increase. This increase was also predicted in Fig. 4(e). This is due to the two consecutive reflections into the skin, i.e., from the quartz–SC interface and SC–epidermis interface. When the SC is thicker, these two reflections are more separated in time, decreasing the destructive interference effect between them and thus increasing the overall P2P amplitude. The dry skin volunteer results still exhibit a clear clustering at the upper right corner (red dots). Finally, in Fig. 5(d), the skin hydration ($H0$) versus SC thickness (d) is shown. From this analysis, it is evident that THz sensing can be utilized to effectively identify dry skin and quantify the effect of moisturizers on the skin. The results in Fig. 8 show how we can follow the process of occlusion dynamically. In this figure, the hydration evolution during the 60 s of the test is shown for nine different volunteers: three with normal skin (a)–(c), three with dry skin (d)–(f), and three with dry skin treated with moisturizer (g)–(i). False color maps are generated for each volunteer. The analysis demonstrates higher initial hydration states for normal skin in contrast with dry skin participants. The participants who previously applied moisturizer have hydration dynamics similar to those with normal skin and so are omitted for clarity.

4 Conclusions

In this research, we have presented the largest *in vivo* study of skin using THz light so far, determining the hydration profile and thickness of the SC of 314 volunteers. With the addition of force sensors to our design, we ensure repeatable and user-independent measurements, enabling robust operation for any potential clinical user. By formulating our own numerical model of the skin, we have demonstrated how the initial hydration state of the skin and the thickness of the SC can be calculated from the occlusion curve. This technique successfully distinguished volunteers with hydrated skin from the ones with dry skin. By running a Student's t-test over the dry and normal skin data, we were able to demonstrate the statistically significant difference between these two groups exhibiting a p-value of 2.46%. While alternative methods for assessing skin hydration such as Raman spectroscopy, OCT, corneometry, and TEWL exist, our THz technique enables the rapid calculation of both skin hydration content and thickness at a rate of 4 Hz. The closest competitor to the THz technique currently in this application is Raman spectroscopy, but the calculation of skin parameters using this method can take up to a minute and the frequencies probed are different. In this work, we are progressing the development of a portable imaging THz scanner, which holds the potential to map hydration levels of specific areas of the skin in real time, positioning THz technology as a highly viable option for clinical use. Based on this research, our future work will focus on studying patients with skin disorders involving abnormalities in the SC, such as eczema, psoriasis, and additionally, skin cancer. We will also investigate the feasibility of increasing the acquisition speed while also increasing the sampled area. Our contribution to this research also opens up the opportunity of using THz techniques to evaluate and guide the development of medical treatments and skin care products in a noninvasive and nondestructive fashion, with far-reaching impact in different fields, including dermatology, epithelial cancer diagnosis, cosmetics, and public health.

5 Appendix: Numerical Modeling of Human Skin

To theoretically model the human skin, as illustrated in Fig. 1(a), we assume that the skin comprises multiple layers, namely, the SC, epidermis, dermis, and subcutaneous tissue. For practical THz examinations, only the SC and a partial region of the epidermis are accessible under THz illumination. These limitations arise from the high absorption coefficient of water (200 cm^{-1} at 1 THz). To model the water distribution in the SC and epidermis, we use an approximated hydration profile acquired using Raman spectroscopy.[35,36] In Fig. 9, the hydration profile is depicted using a continuous black line and its discretization using colored bars.

To model the increasing hydration gradient in the SC (first 15 μm into the skin chosen arbitrarily but optimized afterward for a particular experimental data), a quadratic function is approximated. For the epidermis, a straight line following the SC is fitted. This hydration profile can be fully characterized by only three free parameters: skin surface hydration ($H0$), epidermis hydration ($H1$), and SC thickness (d), illustrated in Fig. 9. Based on previously reported studies using Raman spectroscopy, it has been observed that the epidermis sustains its

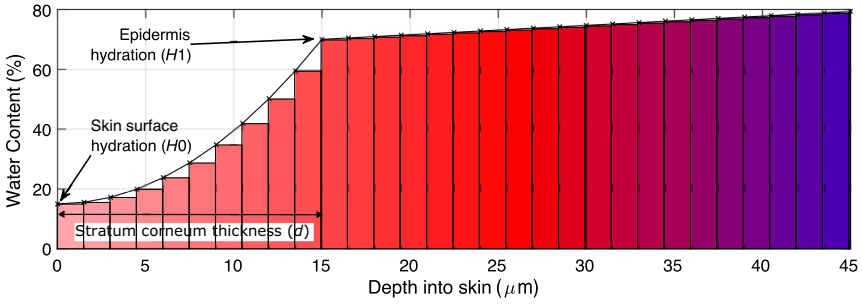

Fig. 9 Numerical modeling of skin. Hydration profile as a function of the skin depth in which the first point, $H0$ is the skin surface hydration, $H1$ is the epidermis hydration, and d is the SC thickness.

hydration even in the presence of a moisturizer agent, and the SC is the only skin layer affected by the presence of water or moisturizer.[35,36] To build our numerical simulations, the hydration profile is subdivided into multiple layers of 2 μm of thickness and constant hydration content. Afterwards, an effective-medium model is used to calculate the effective permittivity of skin under different hydration values given by the staggered hydration profile in Fig. 9,[37]

$$\sum_{i=1}^{J} \eta_i \frac{\epsilon_i - \epsilon_{\text{eff}}}{\epsilon_i + 2\epsilon_{\text{eff}}}, \tag{3}$$

where ϵ_i is the permittivity of the i'th component of the mixture, ϵ_{eff} is the effective permittivity of the mixture, η_i is the volume fraction of the i'th component, and J is the summation of the number of individual components making the mixture. In our particular case, we model the skin as a combination of dry tissue and water. For the permittivity of skin and water, we used Refs. 14 and 38, respectively. This procedure allows us to calculate the complex dielectric properties of the skin as a function of depth. Subsequently, a multilayer model is used to calculate the sum of the multiple reflections in the staggered system depicted in Fig. 9,[37]

$$Z_m = \zeta_m \frac{Z_{m+1} + i\zeta_m \tan(k_m t_m)}{\zeta_m + iZ_{m+1} \tan(k_m t_m)}, \tag{4}$$

where Z_m is the impedance of the m'th sublayer, $\zeta_m = (\omega\mu_m)/k_m$ is the characteristic impedance of the m'th sublayer, and k_m and t_m are the propagation constant and thickness, respectively. This recursive equation allows us to sum the reflection on the different sublayers composing the multilayer system from the deepest layer to the surface. Then, the total reflection seen from the surface and given as

$$\Gamma_0 = \frac{Z_1 - \zeta_0}{Z_1 + \zeta_0}. \tag{5}$$

Finally, recording a THz pulse in the absence of a sample and taking its Fourier transform ($E_0(\omega)$), the simulated reflected pulse is given as

$$E_{\text{sim}}(t) = \text{FFT}^{-1}(\Gamma_0 E_0), \tag{6}$$

where E_0 is a reference THz pulse.[34]

Disclosures

The authors declare no conflict of interest.

Code and Data Availability

The data presented in this article are publicly available on Figshare at https://doi.org/10.6084/m9.figshare.23650791.

Acknowledgments

The authors gratefully acknowledge support from the Engineering and Physical Sciences Research Council (EPSRC) (Grant Nos. EP/S021442/1 and EP/V047914/1), Cancer Research UK, the Royal Society (Wolfson Merit Award-EPM), and the Health GRP at Warwick University.

References

1. P.-G. Sator, J. B. Schmidt, and H. Hönigsmann, "Comparison of epidermal hydration and skin surface lipids in healthy individuals and in patients with atopic dermatitis," *J. Am. Acad. Dermatol.* **48**(3), 352–358 (2003).
2. S. Verdier-Sévrain and F. Bonté, "Skin hydration: a review on its molecular mechanisms," *J. Cosmet. Dermatol.* **6**(2), 75–82 (2007).
3. J. Logger et al., "Noninvasive objective skin measurement methods for rosacea assessment: a systematic review," *Br. J. Dermatol.* **182**(1), 55–66 (2020).
4. A. Byrne, "Bioengineering and subjective approaches to the clinical evaluation of dry skin," *Int. J. Cosmet. Sci.* **32**(6), 410–421 (2010).
5. M. Qassem and P. Kyriacou, "Review of modern techniques for the assessment of skin hydration," *Cosmetics* **6**(1), 19 (2019).
6. I. M. Gidado et al., "Review of advances in the measurement of skin hydration based on sensing of optical and electrical tissue properties," *Sensors* **22**(19), 7151 (2022).
7. F. Novelli, B. Guchhait, and M. Havenith, "Towards Intense THz Spectroscopy on Water: Characterization of Optical Rectification by GaP, OH1, and DSTMS at OPA Wavelengths," *Materials (Basel)* **13**(6), 1311 (2020).
8. A. J. Fitzgerald et al., "Terahertz pulsed imaging of human breast tumors," *Radiology* **239**(2), 533–540 (2006).
9. P. C. Ashworth et al., "Terahertz pulsed spectroscopy of freshly excised human breast cancer," *Opt. Express* **17**(15), 12444–12454 (2009).
10. V. P. Wallace et al., "Terahertz pulsed imaging of basal cell carcinoma *ex vivo* and *in vivo*," *Br. J. Dermatol.* **151**(2), 424–432 (2004).
11. V. P. Wallace et al., "Terahertz pulsed spectroscopy of human basal cell carcinoma," *Appl. Spectrosc.* **60**(10), 1127–1133 (2006).
12. F. Wahaia et al., "Detection of colon cancer by terahertz techniques," *J. Mol. Struct.* **1006**(1-3), 77–82 (2011).
13. D. A. Crawley et al., "Terahertz pulse imaging: a pilot study of potential applications in dentistry," *Caries Res.* **37**(5), 352–359 (2003).
14. G. Hernandez-Cardoso et al., "Terahertz imaging for early screening of diabetic foot syndrome: a proof of concept," *Sci. Rep.* **7**(1), 42124 (2017).
15. K. I. Zaytsev et al., "*In vivo* terahertz pulsed spectroscopy of dysplastic and non-dysplastic skin nevi," *J. Phys. Conf. Ser.* **735**(1), 012076 (2016).
16. S. Sung et al., "THz imaging system for *in vivo* human cornea," *IEEE Trans. Terahertz Sci. Technol.* **8**(1), 27–37 (2017).
17. M. H. Arbab et al., "Terahertz spectroscopy for the assessment of burn injuries *in vivo*," *J. Biomed. Opt.* **18**(7), 077004 (2013).
18. N. Bajwa et al., "Non-invasive terahertz imaging of tissue water content for flap viability assessment," *Biomed. Opt. Express* **8**(1), 460–474 (2017).
19. Q. Sun et al., "*In vivo* estimation of water diffusivity in occluded human skin using terahertz reflection spectroscopy," *J. Biophotonics* **12**(2), e201800145 (2019).
20. J. Wang et al., "THz *in vivo* measurements: the effects of pressure on skin reflectivity," *Biomed. Opt. Express* **9**(12), 6467–6476 (2018).
21. X. Ding et al., "Quantitative evaluation of transdermal drug delivery patches on human skin with *in vivo* THz-TDS," *Biomed. Opt. Express* **14**(3), 1146–1158 (2023).
22. K. Ross and R. Gordon, "Water in malignant tissue, measured by cell refractometry and nuclear magnetic resonance," *J. Microsc.* **128**(1), 7–21 (1982).
23. E. Rofstad et al., "Magnetic resonance imaging of human melanoma xenografts *in vivo*: proton spin—lattice and spin—spin relaxation times versus fractional tumour water content and fraction of necrotic tumour tissue," *Int. J. Radiat. Biol.* **65**(3), 387–401 (1994).
24. E. P. Parrott et al., "Terahertz pulsed imaging *in vivo*: measurements and processing methods," *J. Biomed. Opt.* **16**(10), 106010 (2011).

25. K. I. Zaytsev et al., "Invariant embedding technique for medium permittivity profile reconstruction using terahertz time-domain spectroscopy," *Opt. Eng.* **52**(6), 068203 (2013).
26. C. Baker et al., "Developments in people screening using terahertz technology," *Proc. SPIE* **5616**, 61–68 (2004).
27. M. R. Grootendorst et al., "Use of a handheld terahertz pulsed imaging device to differentiate benign and malignant breast tissue," *Biomed. Opt. Express* **8**(6), 2932–2945 (2017).
28. B. Schulkin et al., "Progress toward handheld THz sensing," in *Int. Conf. Infrared, Millimeter Terahertz Waves*, IEEE, pp. 1–2 (2011).
29. G. J. Wilmink et al., "Development of a compact terahertz time-domain spectrometer for the measurement of the optical properties of biological tissues," *J. Biomed. Opt.* **16**(4), 047006 (2011).
30. Z. B. Harris et al., "Terahertz portable handheld spectral reflection (PHASR) scanners for accurate classification of burn injuries in clinical settings," *Proc. SPIE* **12420**, 1242008 (2023).
31. O. B. Osman et al., "*In vivo* assessment and monitoring of burn wounds using a handheld terahertz hyperspectral scanner," *Adv. Photonics Res.* **3**(5), 2100095 (2022).
32. H. Lindley-Hatcher et al., "Evaluation of *in vivo* THz sensing for assessing human skin hydration," *J. Phys.: Photonics* **3**(1), 014001 (2020).
33. X. Chen and E. Pickwell-MacPherson, "An introduction to terahertz time-domain spectroscopic ellipsometry," *APL Photonics* **7**(7), 071101 (2022).
34. H. Lindley-Hatcher et al., "A robust protocol for *in vivo* THz skin measurements," *J. Infrared, Millimeter Terahertz Waves* **40**, 980–989 (2019).
35. P. Caspers, *In Vivo Skin Characterization By Confocal RAMAN Microspectroscopy*, Erasmus University Rotterdam, Rotterdam (2003).
36. M. Egawa, T. Hirao, and M. Takahashi, "*In vivo* estimation of stratum corneum thickness from water concentration profiles obtained with Raman spectroscopy," *Acta Dermato-Venereol.* **87**(1), 4–8 (2007).
37. D. B. Bennett et al., "Stratified media model for terahertz reflectometry of the skin," *IEEE Sens. J.* **11**(5), 1253–1262 (2010).
38. J. Kindt and C. Schmuttenmaer, "Far-infrared dielectric properties of polar liquids probed by femtosecond terahertz pulse spectroscopy," *J. Phys. Chem.* **100**(24), 10373–10379 (1996).

Arturo I. Hernandez-Serrano received his BSc degree in physics from the University of Guanajuato, Mexico. In 2018, he received his PhD in science (optics) from the Research Centre of Optics, Mexico, where he worked in the design and fabrication of THz devices using 3D printing. In 2018, he joined the MacPherson THz Group at the University of Warwick, UK, in the development of novel methods and devices for the in vivo evaluation of skin diseases using THz spectroscopy.

Xuefei Ding is currently a PhD candidate in physics at the University of Warwick, UK. She received her BE and ME degrees in electrical engineering from Chongqing University, China, in 2018 and 2021, respectively. Her main research interest is developing terahertz spectroscopy techniques for biomedical applications, including *in vivo* evaluation of human skin. She has received the associate fellow of the Higher Education Academy (AFHEA) and the postgraduate certificate in Transferable Skills in Science.

Jacob Young received his master's degree in physics from the University of Bath, where he researched instabilities in fusion plasmas with UKAEA at Culham Centre for Fusion Energy, and neutron detector development with STFC at ISIS. He is currently undertaking a PhD at the University of Warwick, working under Prof. Emma Pickwell-Macpherson to develop in vivo THz medical imaging. This includes developing movement compensation algorithms, modeling human skin, and conducting clinical studies.

Goncalo Costa received his BSc (Hons) degree in mathematics and physics from the University of Dundee in 2020 and his MSc degree in particles, strings, and cosmology from the University of Durham in 2021. He is currently pursuing a PhD at the University of Warwick under the supervision of Prof. Emma Pickwell-MacPherson. His research interests include skin and latex film formation analysis via THz imaging and spectroscopy.

Anubhav Dogra received his PhD in mechanical engineering from the Indian Institute of Technology (IIT) Ropar, Punjab, India. He is currently a post-doctoral research fellow in the MacPherson THz Group working on the Terabotics project, with a focus on integrating robotics with terahertz. His research interests include the design and development of robotics systems particularly in manipulation, modular robotics, medical robotics, and multibody dynamics.

Joseph Hardwicke is a consultant in plastic and reconstructive surgery, the director of the Institute of Applied and Translational Technologies in Surgery at the University Hospitals of Coventry and Warwickshire NHS Trust (UHCW), an honorary professor at the University of Warwick, and a visiting professor at Coventry University. His research focuses on clinical trials of novel technologies and their translational into everyday clinical care, through research-based assessment bound within a high-quality governance system.

Emma Pickwell-MacPherson received her PhD in biomedical applications of THz spectroscopy and imaging with the Semiconductor Physics Group, Cambridge University, and TeraView Ltd., a company specializing in terahertz imaging, in 2002. She is a professor at Warwick University in the Physics Department in the Ultrafast Photonics Group. She is PI of the £8M EPSRC Programme grant, "Terabotics," which combines advances in THz technology and surgical robotics.